Emergence of Complex Coordination Clusters $\{Cu^{II}_{48}Na_{12}\}$ by Using Multiple Ligands under Oxidizing Conditions

Wei Meng,[a,b] Hongfang Ye,[a] Shuai Liu,[a] FengXu*[a] and Weijian Xu[a]

[a] State Key Laboratory for Chemo/Biosensing and Chemometrics, College of Chemistry & Chemical Engineering, Hunan University, Changsha, 410082, P. R. China

[b] Hunan Provincial Key Lab of Dark Tea and Jin-hua, Department of Materials & Chemistry Engineering, Hunan City University, Yiyang, 413000, P. R. China

Table of Contents

I. Experimental Section S2

II. X-Ray Crystallographic Analysis S3

III. Supplementary Physical Characterization S4-S13

IV. Supplementary Structural Figures S14-S18

V. References S19

I. Experimental Section

1. Materials and Methods:

All of the reactants were reagent grade and used as purchased. IR spectra were measured on PerkinElmer Spectrum 100 FT-IR spectrometer and Brucker TENSOR II FTIR Spectrometer. Thermogravimetric analysis (TGA) measurements were carried out using a DSC/TG pan A1203 system in N_2 flow with a heating rate of 10 ℃ min^{-1}. Elemental analyses were performed (C, H, N) by Thermo Scientific FLASH 2000 elemental analyzer; Cu, Na and P were analyzed on a Varian (720) ICP atomic emission spectrometer. Powder X-ray diffraction (PXRD) patterns were collected at room temperature on a Rigaku D/Max 2500 diffractometer. Magnetic susceptibility measurements were made using a Quantum Design Physical Property Measurement System (QD-PPMS) in the temperature range 2−300 K with an applied field of 1000 Oe. Field-dependent magnetization was recorded at 2 K. ^{13}C-NMR spectra were recorded on a Bruker Avance (100 MHz for ^{13}C-NMR). The XPS analyses were performed with a Thermo Scientific Escalab 250 spectrometer using a focused monochromatized Al Kα radiation (hv = 1486.6 eV). The pressure in the analysis chamber was ca. 2×10^{-9} mbar. Dynamic light scattering (DLS) measurements were taken using the Malvern Zetasizer Nano ZS. The EPR measurements were carried out on a Bruker E500 instrument operating in the X-band and equipped with an Oxford cryostat working in the temperature range of 4-298 K. The samples (40 mg) were placed into a spectroscopically pure quartz cell and sent into the ESR cavity with fixed depth. The solid-state CD spectra were measured on MOS-500 Spectrometer. The morphology of all materials was investigated by scanning electron microscope (SEM, Hitachi, S-4800). We found that ^{13}C-NMR of L-**1** in D_2O showed no obvious signals, which should be caused by the presence of the paramagnetic Cu(II) ions. Therefore, to rule out the effect of Cu(II) ions, Na_2S was added into the L-**1**/D_2O solution. The as-formed black precipitate, CuS, were then filtered out, while the colorless filtration was used for further ^{13}C-NMR test. In the acquired spectrum of this colorless filtration now containing only organic components from the cluster, two new peaks, 177.4 and 82.4 ppm, in the acquired spectrum can be observed, compared with the spectrum of the mixture of L-tart, NaOAc and Na_2CO_3. This result is in consistent with the predicted paramagnetically shifted resonances of C_6 anions. Additionally, a few less obvious signals may be noticed, which can be ascribed to a few facts including C_6 is not the most stable compound and the ^{13}C-NMR measurement can take some time.[1] Ferroelectric were measured on Precision LC ferroelectric tester, Radiant Technologies, inc.

2. Synthesis of L-1 and D-1:

L-**1**: A mixture of $Cu(OAc)_2\cdot H_2O$ (199 mg, 1 mmol), L-(+)-tartaric acid (150 mg, 1 mmol) and Na_2HPO_4 (71 mg, 0.5 mmol) was dissolved in a sodium acetate/acetic acid buffer solution (pH 5.5, 0.5 M NaOAc/HOAc, 10 mL). Gradually added in K_2CO_3 (4 ml, 2 M) while stirring. The mixture was stirred at room temperature for 6 h, then the

resulting blue-yellow solution was filtered and the filtrate was left undisturbed at ambient temperature. After several days, the blue needle crystals were obtained by filtration, washed with MeOH and dried under vacuum. The yield is 10% based on copper. Anal. calcd for $C_{126}H_{90}Cu_{48}Na_{12}O_{236}P_2$ (L-**1**): C 17.25, H 1.03, P 0.71, Cu 34.76, Na 3.15. Found: C 17.30, H 1.07, P 0.61, Cu 34.68, Na 3.12. IR (KBr, cm^{-1}): 3440 s, 2363 w, 2156 w, 1935 w, 1640 s, 1485 m, 1353 s, 1116 m, 1087 s, 1043 s, 962 m, 932 m, 851 m, 815 m, 762 m, 642 m, 563 m, 512 w, 468 m, 423 w.

D-**1** was prepared in a similar fashion to L-**1** except that D-(-)-tartaric acid was used instead of L-(+)-tartaric acid (yield 10 % based on copper). Anal. calcd for $C_{126}H_{90}Cu_{48}Na_{12}O_{236}P_2$ (D-**1**): C 17.25, H 1.03, P 0.71, Cu 34.76, Na 3.15. Found: C 17.17, H 1.10, P 0.65, Cu 34.60, Na 3.01. IR (KBr, cm^{-1}): 3440 s, 2363 m, 1935 w, 1648 s, 1486 m, 1352 s, 1117 m, 1082 s, 1044 s, 963 m, 926 m, 852 m, 822 m, 764 m, 646 m, 563 m, 513 w , 469 m, 418 w.

II. X-Ray Crystallographic Analysis

Table S1. Crystal data and structure refinement for complexes L-**1** and D-**1.**

complexes	L-**1** (1445088)	D-**1** (1469286)
empirical formula	$C_{63}H_{45}Cu_{24}Na_6O_{118}P$	$C_{63}H_{45}Cu_{24}Na_6O_{118}P$
fw	4383.86	4383.86
cryst syst	Hexagonal	Hexagonal
space group	$P6_322$	$P6_322$
a [Å]	30.1147(9)	29.9131(9)
b [Å]	30.1147(9)	29.9131(9)
c [Å]	29.3170(16)	29.3520(16)
α [deg]	90	90
β [deg]	90	90
γ [deg]	120	120
V [$Å^3$]	23025.4(19)	22745.3(18)
Z	4	4
Dcalcd [g/cm^{-3}]	1.265	1.280
μ [mm^{-1}]	2.259	2.286
F(000)	8576.0	8576.0
Flack parameter	0.53(2)	0.47(3)
goodness-of-fit on F^2	0.855	1.035
R indices (all data)	R_1 = 0.0623(9127) wR_2 = 0.1936(11028)	R_1 = 0.0541 wR_2 = 0.1781

The data were collected at 100 K at 3W1A of the Beijing Synchronic Radiation Facility with λ = 0.70 Å radiation. The data were reduced by HKL 2000.[2] The structures of L-**1** and D-**1** were solved by the direct method and refined by the full-

matrix least-squares method on F^2 using the SHELXTL-97 crystallographic software package.[3] Crystallographic data and structural refinements for compounds L-**1** and D-**1** are summarized in Table S1. More details on the crystallographic studies as well as atomic displacement parameters are given in the CIF files. All carbon-bonded hydrogen atoms were placed in geometrically calculated positions; hydrogen atoms in water molecules were not assigned or directly included in the molecular formula.

III. Supplementary Physical Characterization

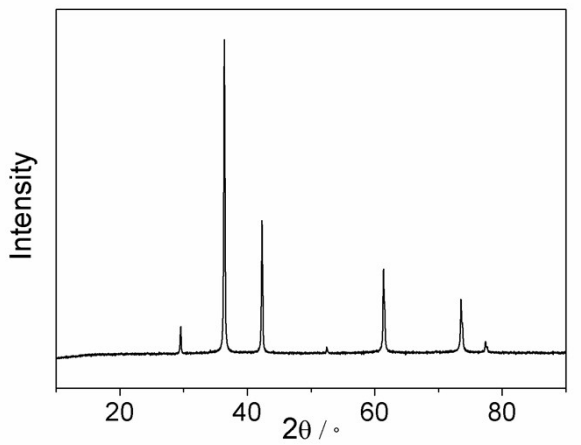

Figure S1. Observed powder X-ray diffraction (PXRD) of Cu_2O.

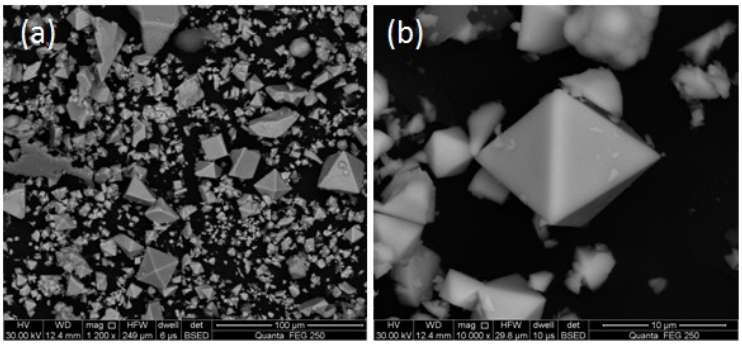

Figure S2. SEM images of Cu_2O octahedra.

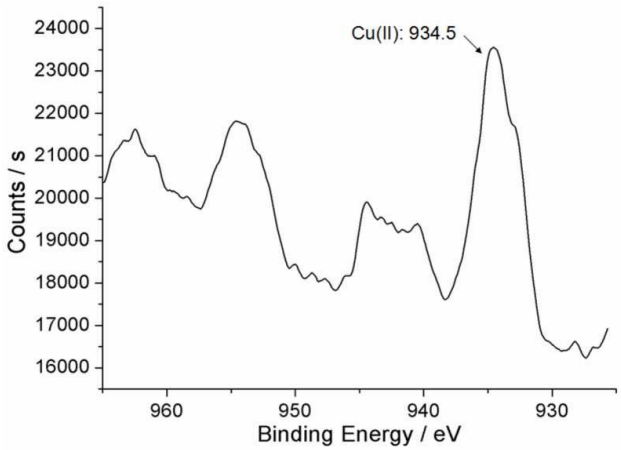

Figure S3. The XPS of L-**1.**

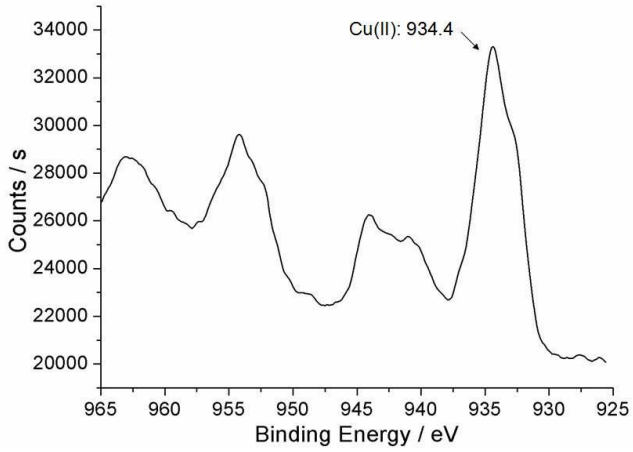

Figure S4. The XPS of D-**1.**

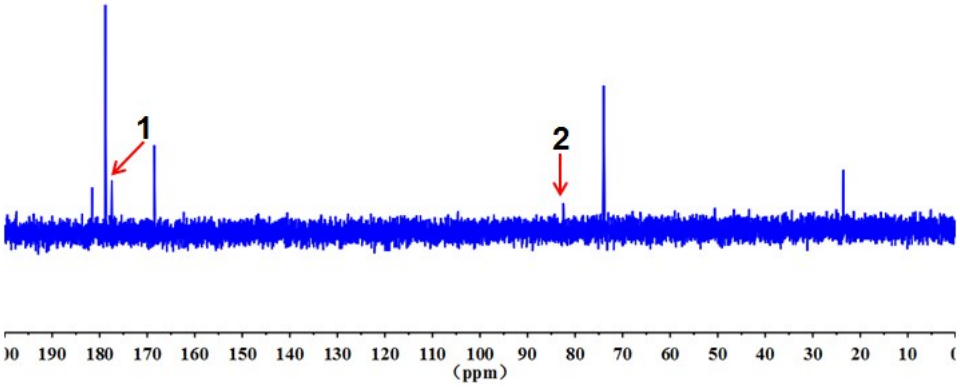

Figure S5. The D-**1** samples suitable for ^{13}C-NMR studies were prepared by dissolving single crystals in D_2O, followed by the addition of Na_2S and filtration. Compared with the spectrum of the mixture of D-tart, NaOAc and Na_2CO_3, two new peaks appeared at 177.4 and 82.4 ppm.

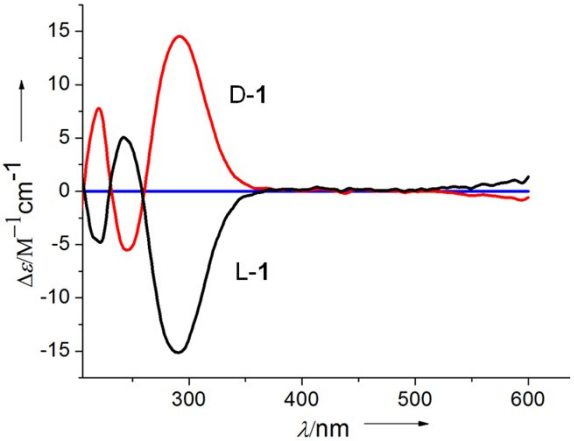

Figure S6. CD spectra of L-**1** and D-**1** in a 0.5 M NaOAc/HOAc buffer solution at pH 5.5.

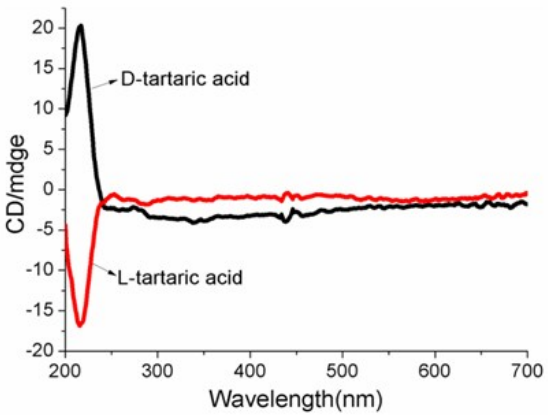

Figure S7. The solid-state CD spectra of L-(+)- and of D-(-)-tartaric acid.

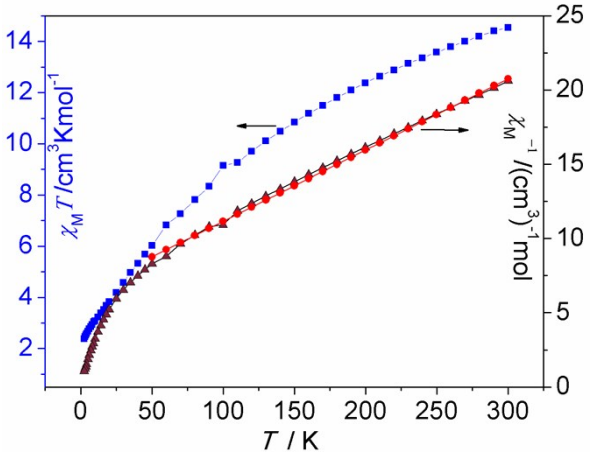

Figure S8. $\chi_M T$ and χ_M^{-1} vs T plots of compounds D-**1** in the temperature range 2.5 ~ 300 K at the field of 1000 Oe. The red solid line present the fitting results of D-**1** with the modified Curie-Weiss law.

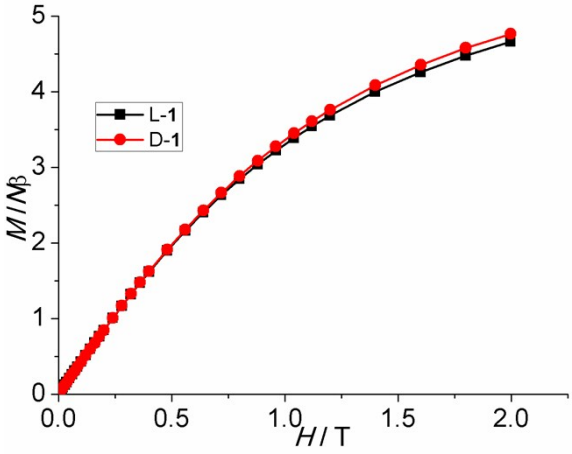

Figure S9. Magnetization vs external magnetic field for L-**1** and D-**1** at 2 K.

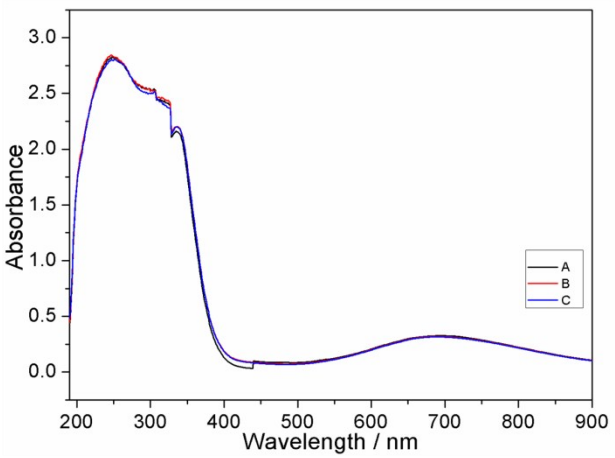

Figure S10. The UV-Vis spectra of L-**1** in the wavelength range of 190 ~ 900 nm. The UV-Vis spectrum (A to C) were detected per 12 hours for three times in H_2O.

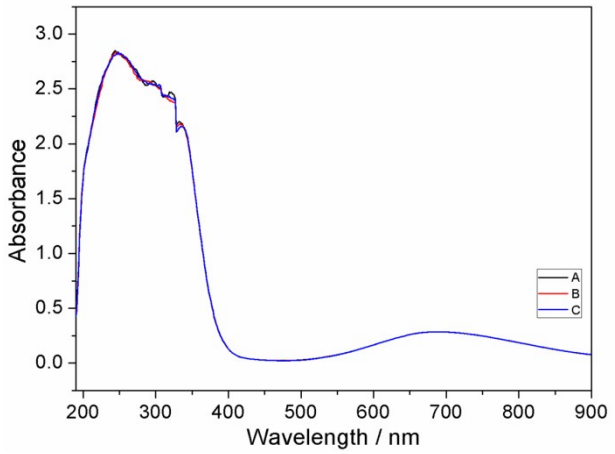

Figure S11. The UV-Vis spectra of D-**1** in the wavelength range of 190 ~ 900 nm. The UV-Vis spectrum (A to C) were detected per 12 hours for three times in H_2O.

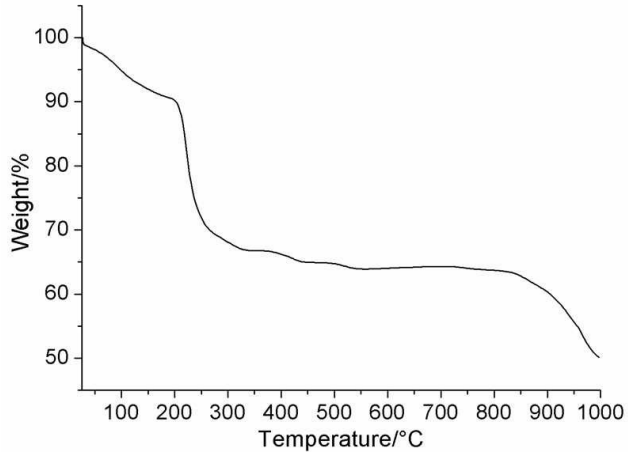

Figure S12. TGA of L-**1** in the N_2 flow.

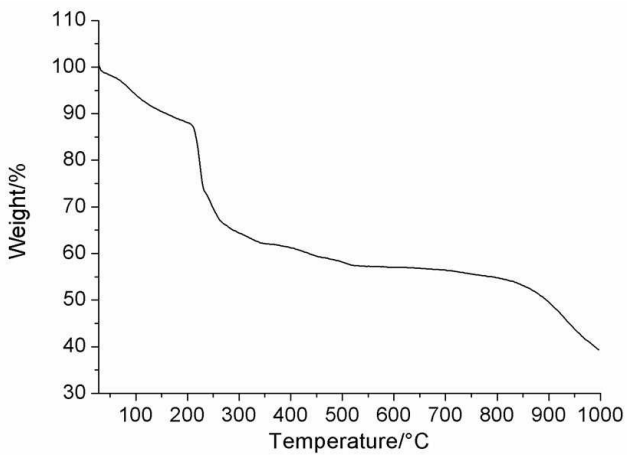

Figure S13. TGA of D-**1** in the N_2 flow.

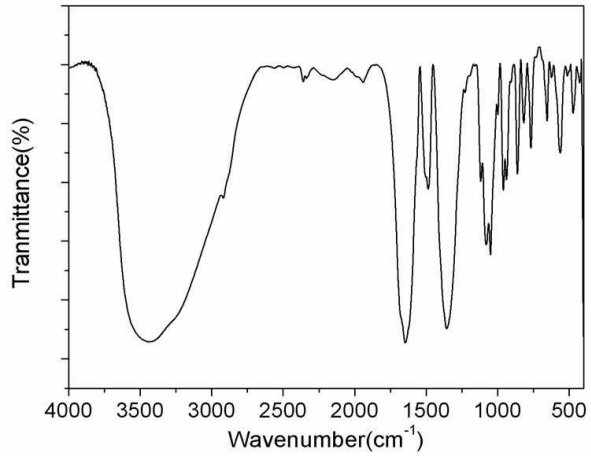

Figure S14. IR spectrum of L-**1**.

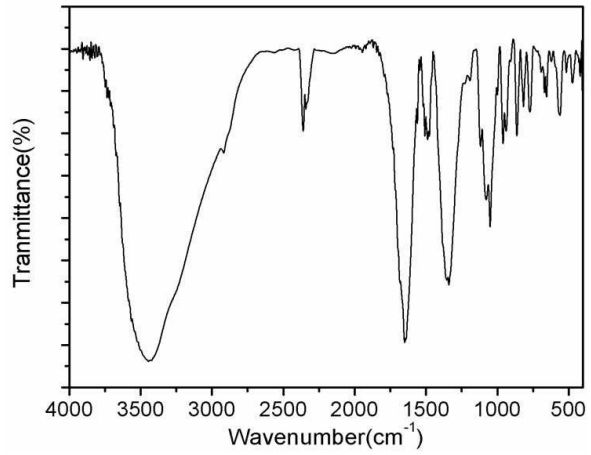

Figure S15. IR spectrum of D-**1**.

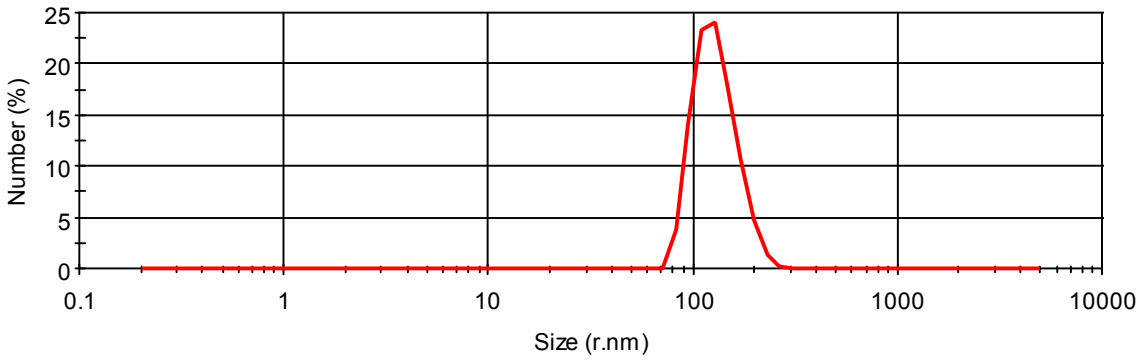

Figure S16. Size distribution by number of nanoparticles for 0.1 mM L-**1** aqueous solution.

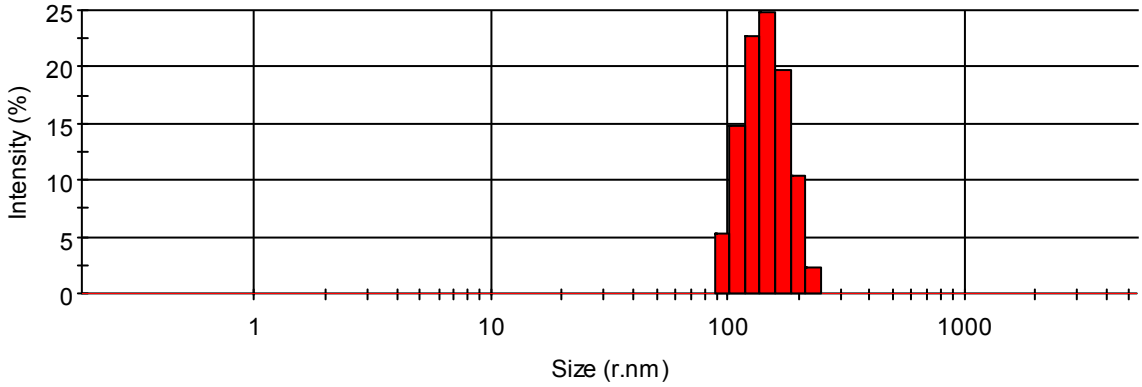

Figure S17. Hydrodynamic radii for 0.1 mM L-**1** aqueous solution.

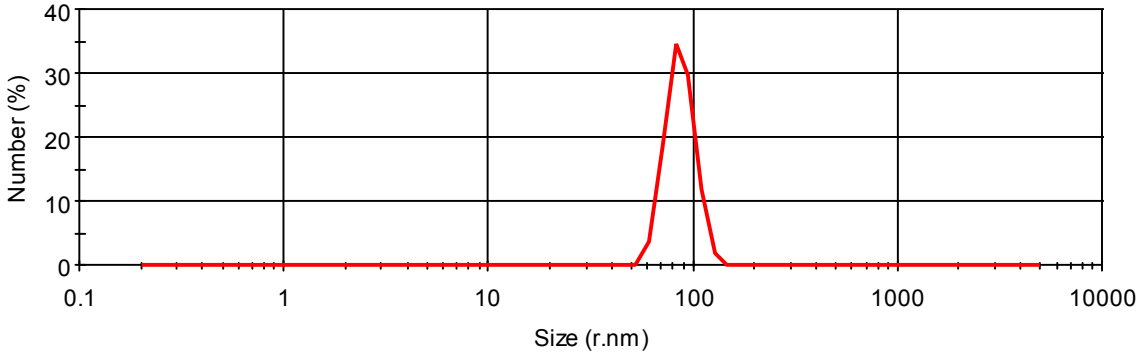

Figure S18. Size distribution by number of nanoparticles for 0.1 mM L-**1** aqueous solution after 48 hours.

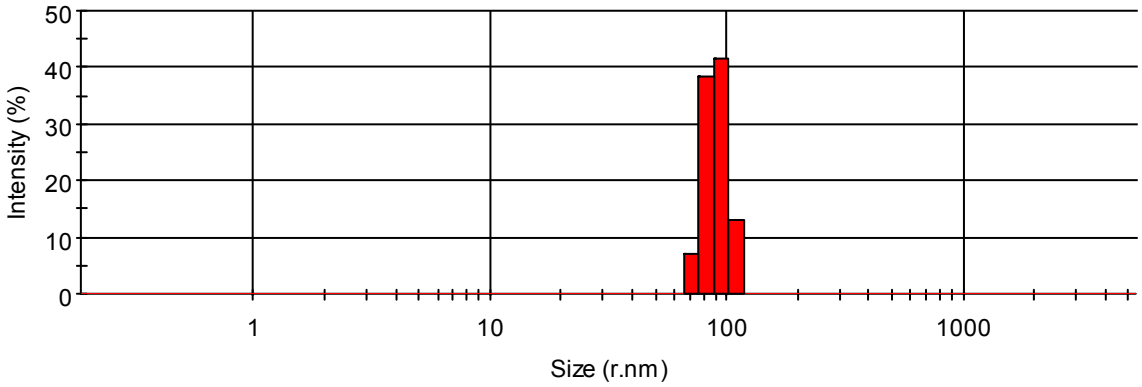

Figure S19. Hydrodynamic radii for 0.1 mM L-**1** aqueous solution after 48 hours.

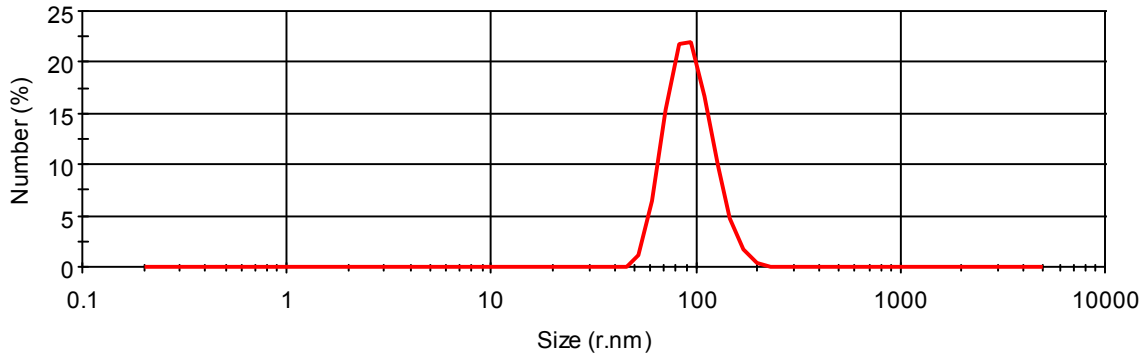

Figure S20. Size distribution by number of nanoparticles for 0.1 mM D-**1** aqueous solution.

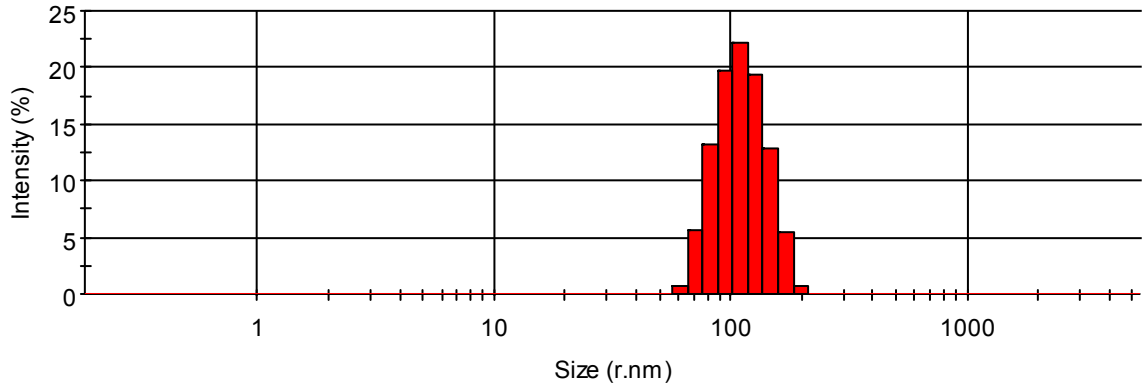

Figure S21. Hydrodynamic radii for 0.1 mM D-**1** aqueous solution.

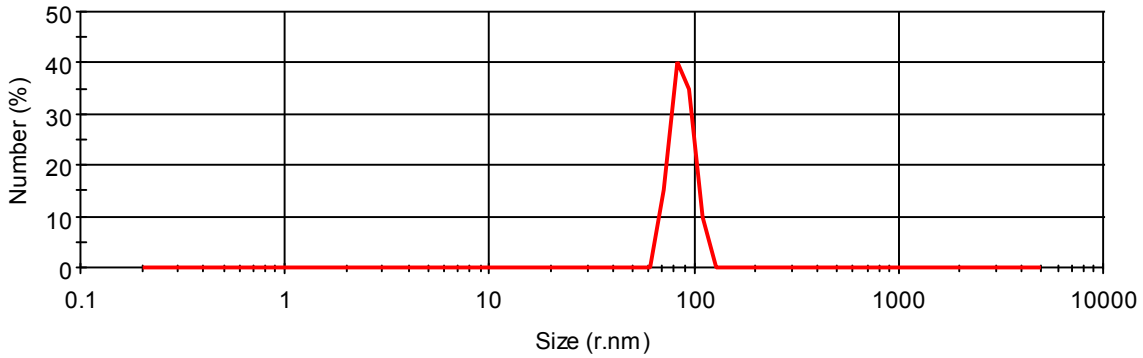

Figure S22. Size distribution by number of nanoparticles for 0.1 mM D-**1** aqueous solution after 48 hours.

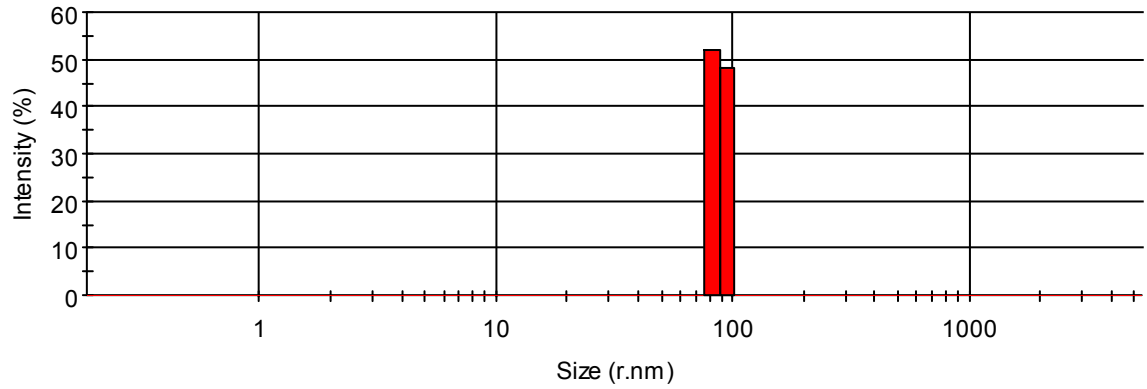

Figure S23. Hydrodynamic radii for 0.1 mM D-**1** aqueous solution after 48 hours.

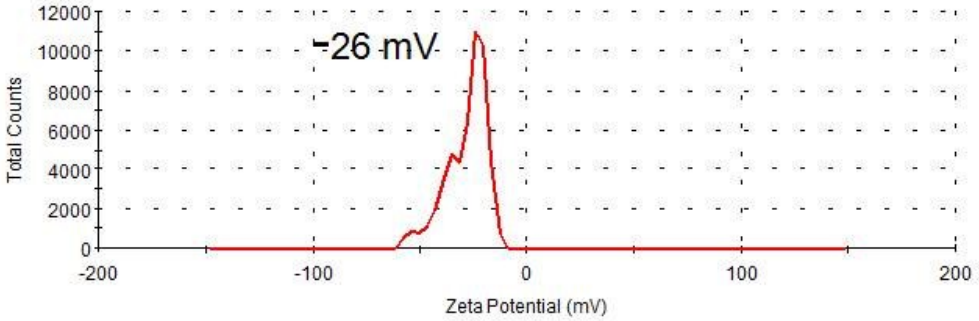

Figure S24. The zeta potential distribution for 0.1 mM L-**1** aqueous solution.

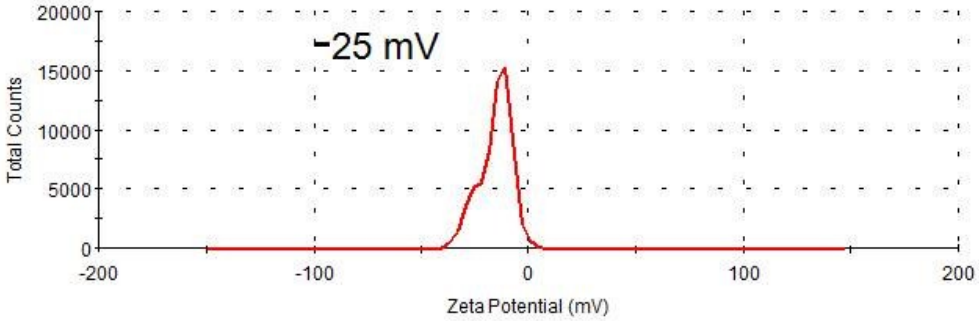

Figure S25. The zeta potential distribution for 0.1 mM L-**1** aqueous solution after 48 hours.

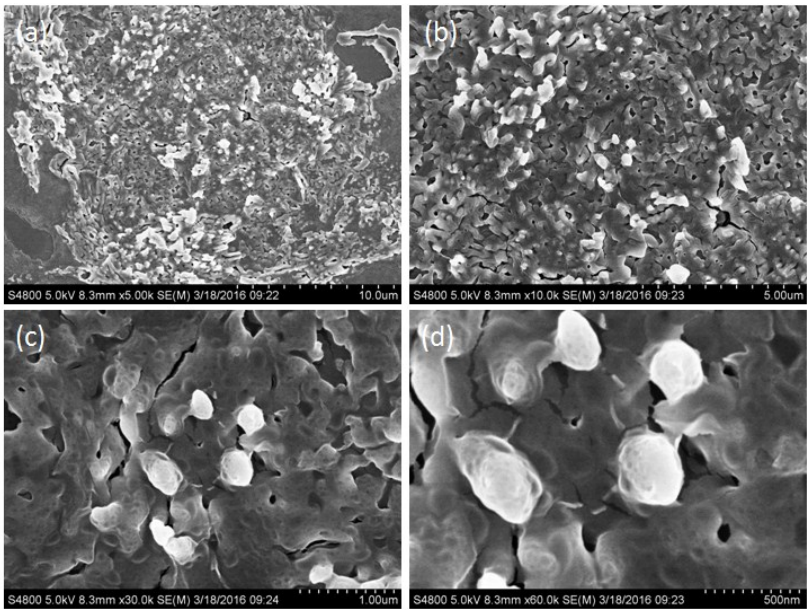

Figure S26. SEM images of L-**1**.

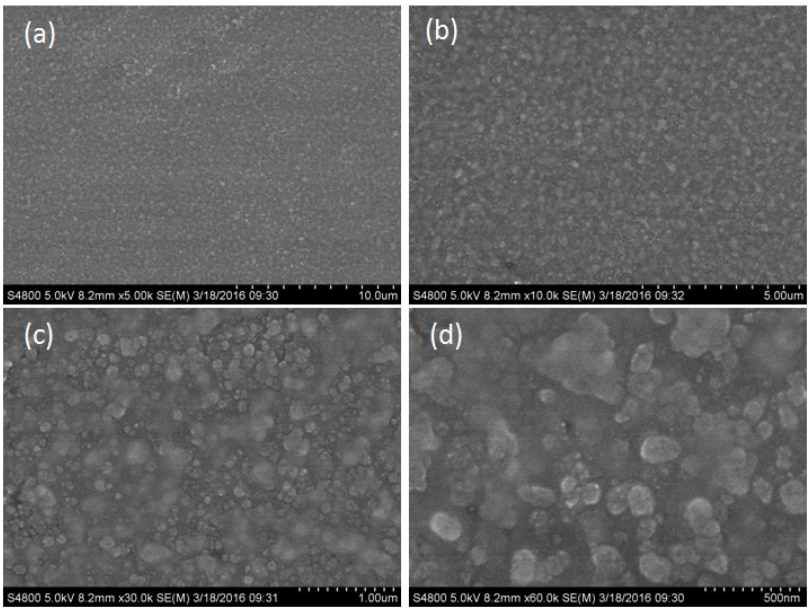

Figure S27. SEM images of D-**1**.

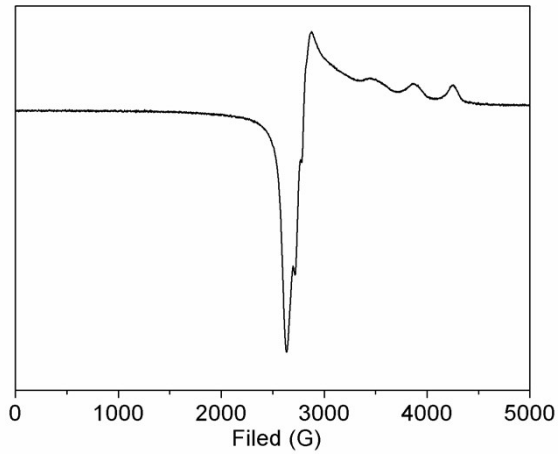

Figure S28. X-band EPR spectrum of L-**1** powder sample at 100 K.

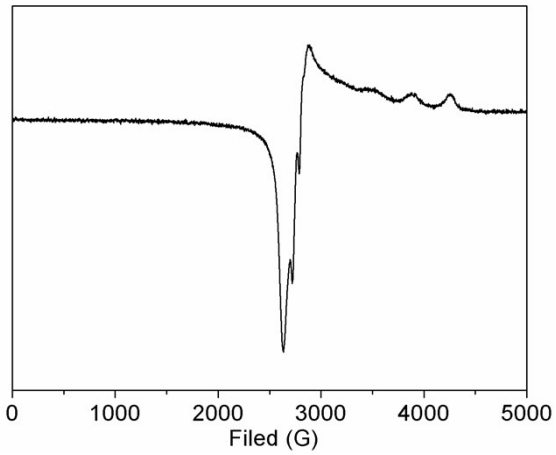

Figure S29. X-band EPR spectrum of D-**1** powder sample at 100 K.

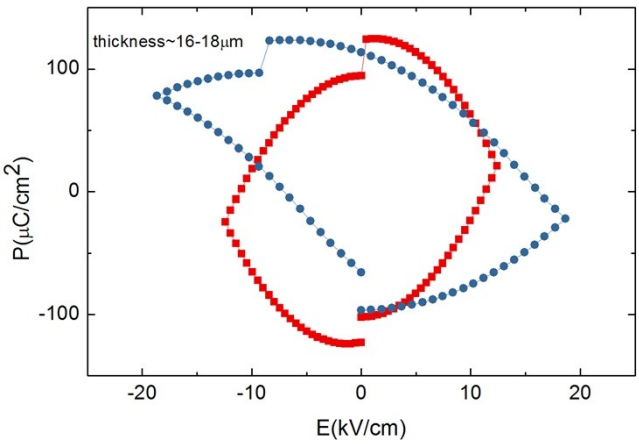

Figure S30. Electric hysteresis loop for L-**1** at room temperature, observed for a single-crystal sample using a ferroelectric tester. The curves are very fat and basically no polarity reversal is observed the samples are very leaky that the ferroelectric feature, if there is any, is masked.

IV. Supplementary Structural Figures

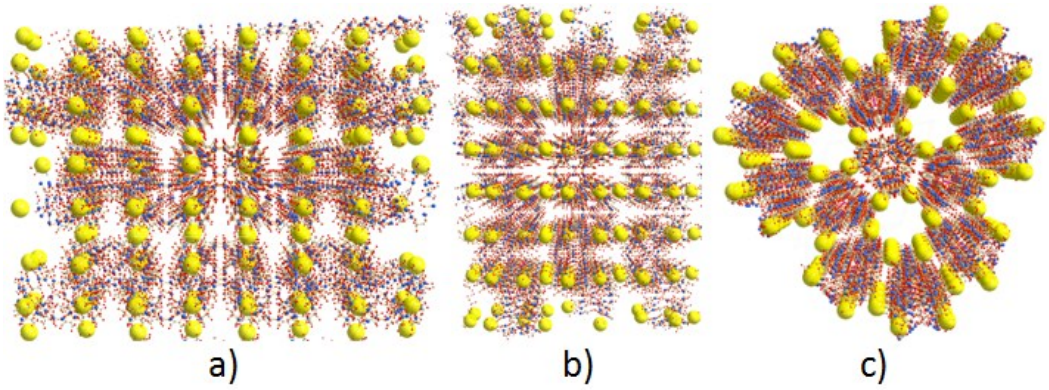

Figure S31. Through the $C_6\cdots Na^+$ interactions, each discrete $\{Cu_{48}Na_9\}$ cluster, in turn, is interlinked to its nearest six $\{Cu_{48}Na_9\}$ neighbors to build a three-dimensional supramolecular framework along (a) a-axis, (b) b-axis, (c) c-axis. Color code: Cu blue, Na yellow, O red, C gray, hydrogen atoms omitted for clarity.

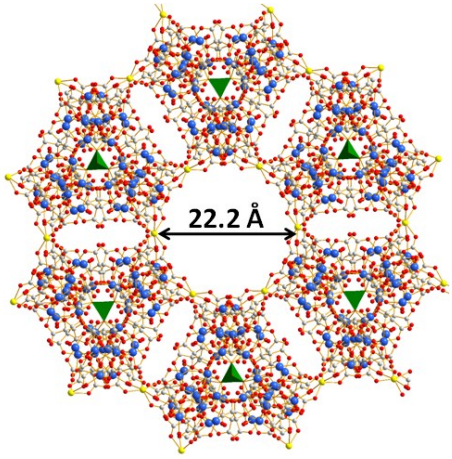

Figure S32. Three-dimensional supramolecular framework of $\{Cu_{48}Na_9\}$ containing pore canals with diameters of 22.2 Å. Color code: Cu blue, Na yellow, O red, C gray, hydrogen atoms omitted for clarity.

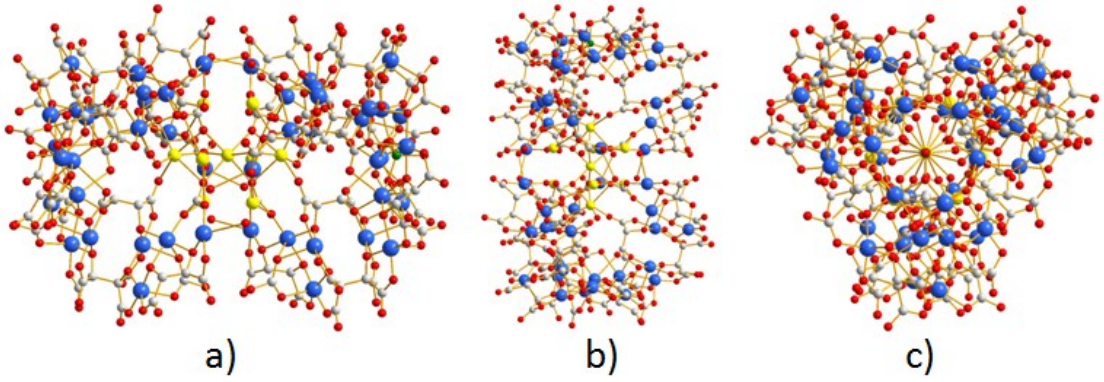

Figure S33. Ball-and-stick representations of L-**1** clusters along (a) a-axis, (b) b-axis, (c) c-axis. Color code: Cu blue, Na yellow, O red, C gray, hydrogen atoms omitted for clarity.

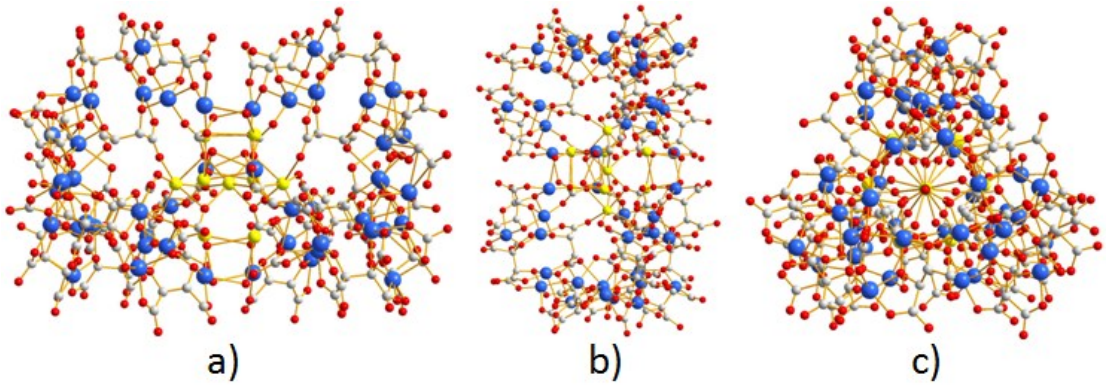

Figure S34. Ball-and-stick representations of D-**1** clusters along (a) a-axis, (b) b-axis, (c) c-axis. Color code: Cu blue, Na yellow, O red, C gray, hydrogen atoms omitted for clarity.

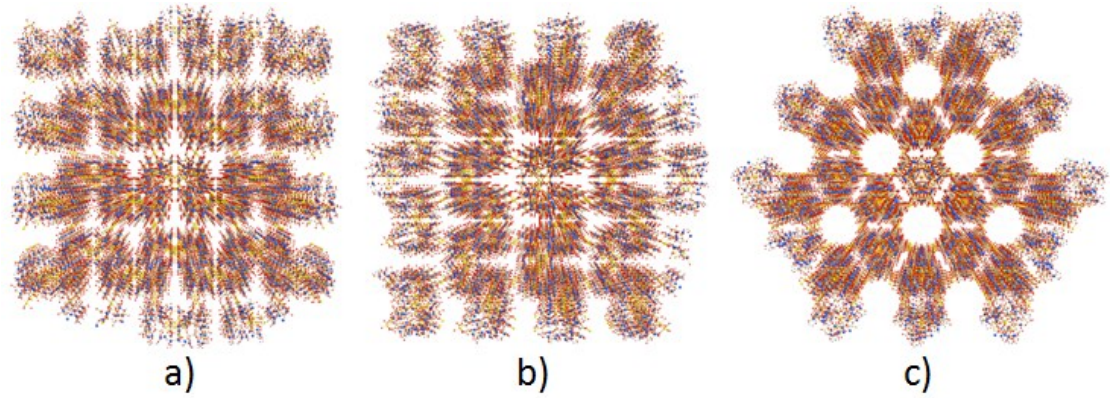

Figure S35. Ball-and-stick representation of 3D supramolecular of L-**1** along (a) a-axis, (b) b-axis, (c) c-axis. Color code: (Cu blue, Na yellow, O red, C gray, hydrogen atoms omitted for clarity.

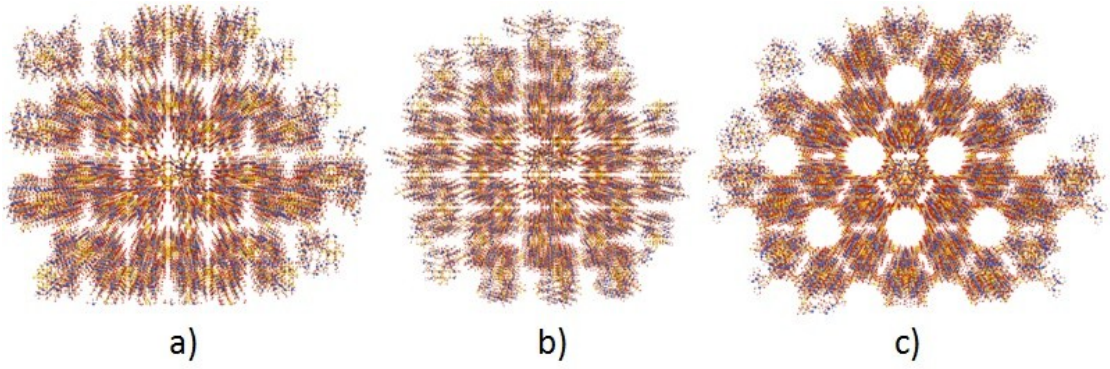

Figure S36. Ball-and-stick representation of 3D supramolecular of D-**1** along (a) a-axis, (b) b-axis, (c) c-axis. Color code: Cu blue, Na yellow, O red, C gray, hydrogen atoms omitted for clarity.

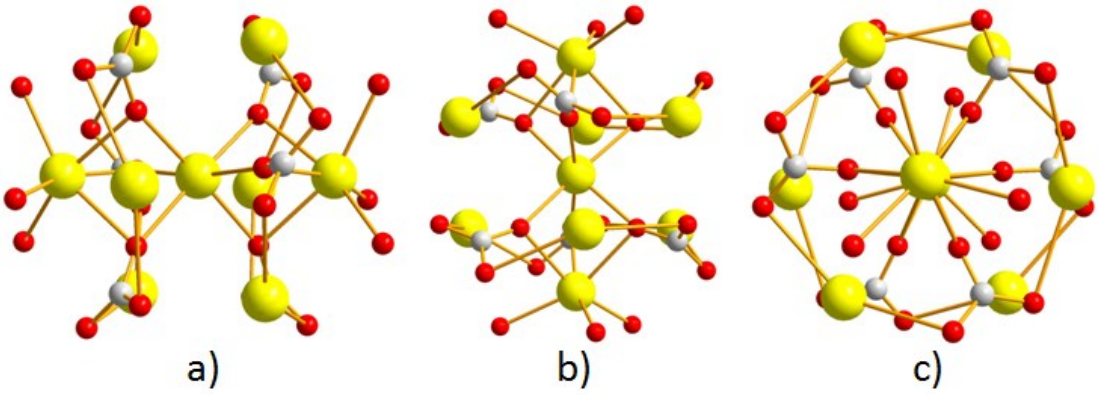

Figure S37. Ball-and-stick representations of {Na_9} clusters along (a) a-axis, (b) b-axis, (c) c-axis. Color code: Na yellow, O red, C gray, hydrogen atoms omitted for clarity.

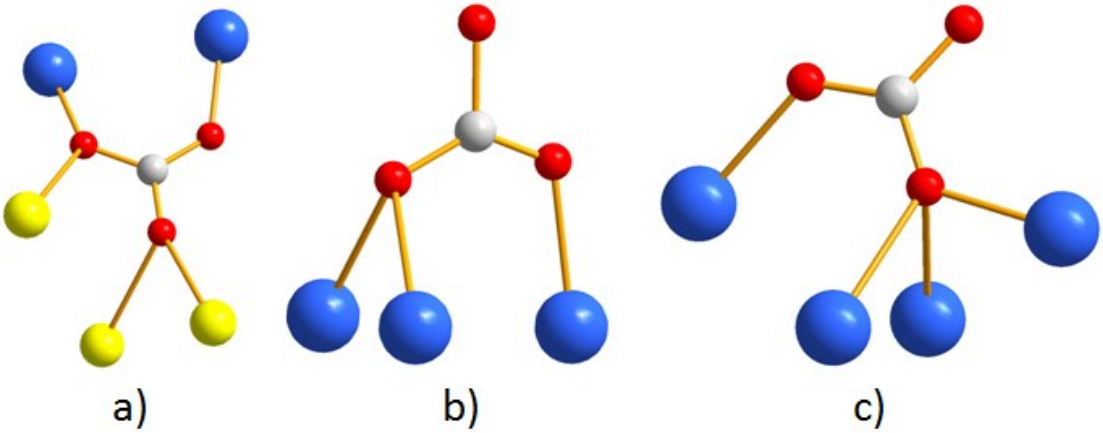

Figure S38. Schematic view of three coordination modes of the CO_3^{2-}. (a) 5.122 in subunit- γ, (b) 3.12 in subunit- γ, (c) 4.13 in subunit-β. Color code: Cu blue, Na yellow, O red, C gray, hydrogen atoms omitted for clarity.

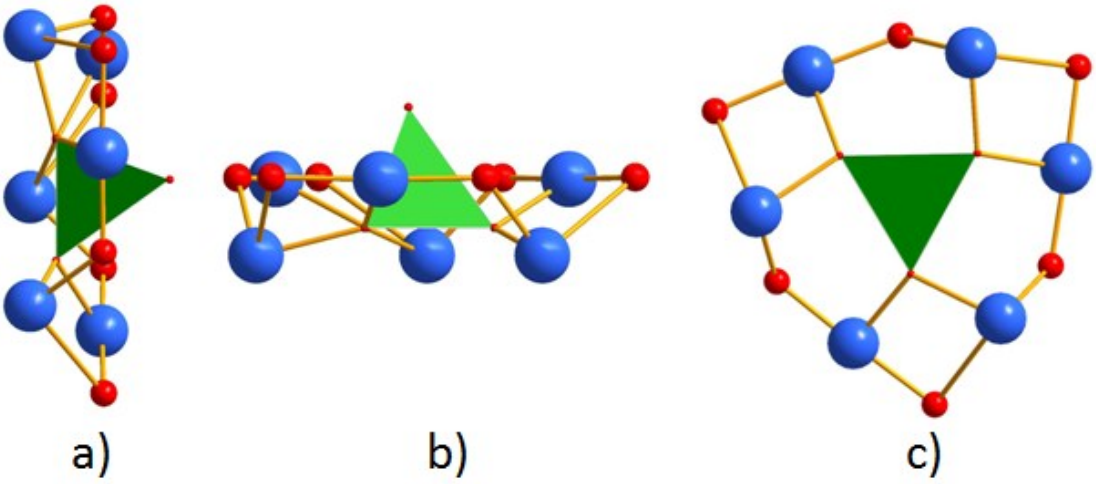

Figure S39. Schematic view of coordination mode of the PO_4^{3-} in a κ^3-(*O*,*O*,*O*) fashion along (a) a-axis, (b) b-axis, (c) c-axis. Color code: Cu blue, O red, P green, hydrogen atoms omitted for clarity.

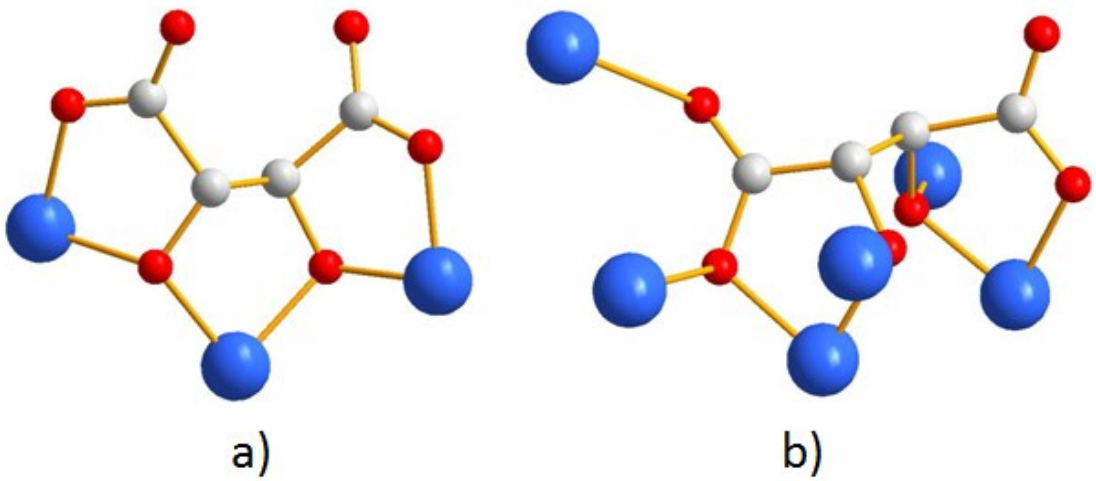

Figure S40. Schematic view of two coordination modes of the tartrate ligands in D-**1**. Color code: Cu blue, Na yellow, O red, C gray, hydrogen atoms omitted for clarity.

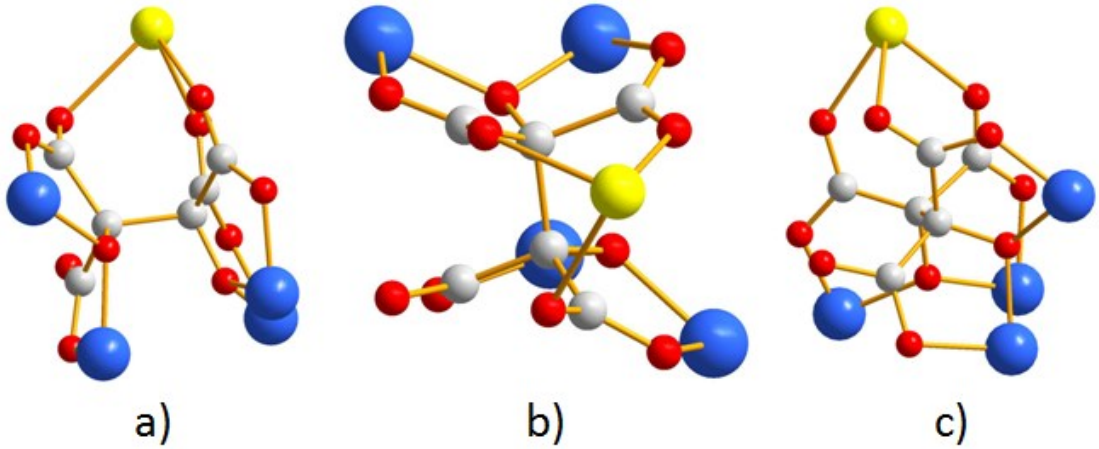

Figure S41. Ball-and-stick representations of C_6 along (a) a-axis, (b) b-axis, (c) c-axis. Color code: Cu blue, Na yellow, O red, C gray, hydrogen atoms omitted for clarity.

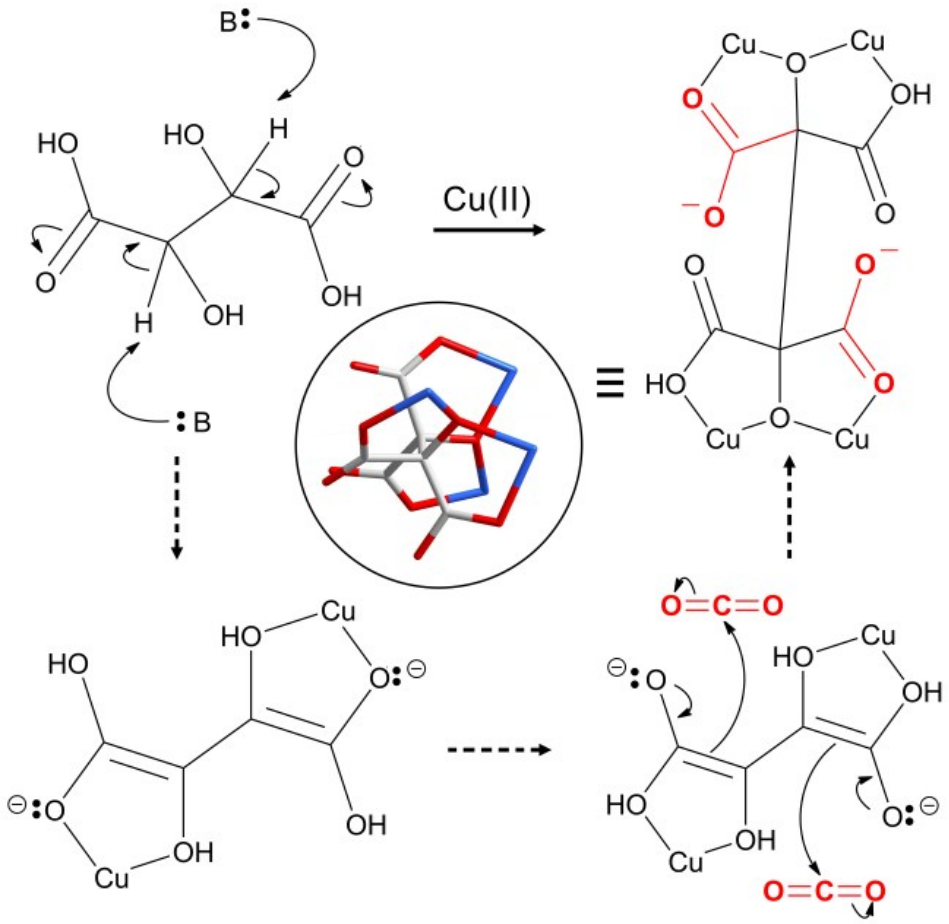

Figure S42. Proposed Formation Mechanism of the C_6 anion.

V. References

1. Pascu, G.; Deville, C.; Clifford, S. E.; Guenée, L.; Besnard, C.; Krämer, K. W.; Liu, S.; Decurtins, S.; Tuna, F.; McInnes, E. J. L.; Winpenny, R. E. P.; Williams, A. F. *Dalton Trans.* **2014**, *43*, 656-662.
2. Otwinowski, Z.; Minor, W. *Methods in Enzymology* (Eds.: C. W. Carter Jr., R. M. Sweet), Academic Press, New York, **1997**, vol. 276, part A, p. 307-326.
3. Sheldrick, G. M. *SHELXL97, Program for Crystal Structure Refinement*, University of Göttingen: Göttingen, Germany, **1997**.